ADVANCED FUNCTIONAL MATERIALS
www.afm-journal.de

Precisely Coordination-Modulated Ultralong Organic Phosphorescence Enables Biomimetic Fluorescence-Afterglow Dual-Modal Information Encryption

Guangqiang Yin, Guifei Huo, Min Qi, Depeng Liu, Longqiang Li, Jiayin Zhou, Xiaoxia Le, Yu Wang, and Tao Chen**

Information leakage and counterfeiting are serious worldwide issues that tremendously impact legitimate businesses and human life. Inspired by the Noctiluca scintillans, a new fluorescence-afterglow dual-modal information encryption enabled by precisely coordination-modulated ultralong organic phosphorescence (UOP) is presented. Strikingly, the optical properties including fluorescence, lifetime and intensity of UOP can be precisely modulated on-demand through energy transfer by lanthanide (Ln^{III}) coordination, which enables information camouflage by similar Ln^{III} luminescence to provide misleading information along with data decryption in the form of mutual afterglow. Moreover, the important data can be encrypted in a spatial-time-resolved way by programmatically coding information with afterglow gradients, yielding greatly improved security for verifying the authenticity. This study provides a new avenue to precisely modulate the optical properties of UOP materials and broadens the scope of optical materials for innovative information encryption and anticounterfeiting applications.

1. Introduction

In the era of the information explosion, information leakage and counterfeiting have already become worldwide issues that pose a severe threat to human health, social security and the economy.[1] It was estimated by Frontier Economics that the global economic loss caused by counterfeiting and piracy would amount to $2.3 trillion by 2022.[2] What's even more concerning, is that counterfeit medicines account for ≈10% of total medicine worldwide, which have disastrous implications on more than one million people annually according to the World Health Organization.[3] Over the past several decades, the development of advanced optical materials and technologies has flourished to combat the escalating challenge posed by fake information and counterfeit behaviors. A myriad of well-known optical materials and technologies have been explored and utilized to encrypt data, such as fluorescence-tag-based techniques,[4] laser holograms,[5] watermarks,[6] and so on. However, these conventional optical technologies still suffer a great risk of being decrypted or duplicated because they are well-established systems based on spatial-resolved variations.[7] Thus, developing innovative unclonable optical materials and cryptographic techniques are urgently needed to achieve higher security for information storage and dissemination.

Lanthanide (Ln^{III})-doped materials have shown considerable promise in information encryption and anticounterfeiting owing to their outstanding luminescent properties including large Stokes shift, narrow spectral lines, high quantum yields, and excellent photostability.[8] Therefore, Ln^{III}-doped materials are finely used in Chinese RMB and Euro banknotes as emissive anti-counterfeiting labels to offer characteristic luminescence under UV irradiation.[9] Unfortunately, the Ln^{III} emissions are based on their inherent f–f transitions, which lead to a high risk of being duplicated. On this basis, we consider whether it is possible to introduce an additional time dimension for Ln^{III} luminescence to further enhance the security level of anti-counterfeiting and improve the capacity and crypticity for information storage.

G. Yin, M. Qi, D. Liu, L. Li, J. Zhou, X. Le, T. Chen
Key Laboratory of Marine Materials and Related Technologies
Zhejiang Key Laboratory of Marine Materials and Protective Technologies
Ningbo Institute of Materials Technology and Engineering
Chinese Academy of Sciences
Ningbo 315201, China
E-mail: lexiaoxia@nimte.ac.cn; tao.chen@nimte.ac.cn
G. Yin, M. Qi, D. Liu, L. Li, J. Zhou, X. Le, T. Chen
School of Chemical Sciences
University of Chinese Academy of Sciences
Beijing 100049, China
G. Huo
Department of Chemistry
National University of Singapore
Singapore 117543, Singapore
Y. Wang
Shanghai Yuking Water Soluble Material Tech Co., Ltd.
Shanghai 200120, China

The ORCID identification number(s) for the author(s) of this article can be found under https://doi.org/10.1002/adfm.202310043

DOI: 10.1002/adfm.202310043

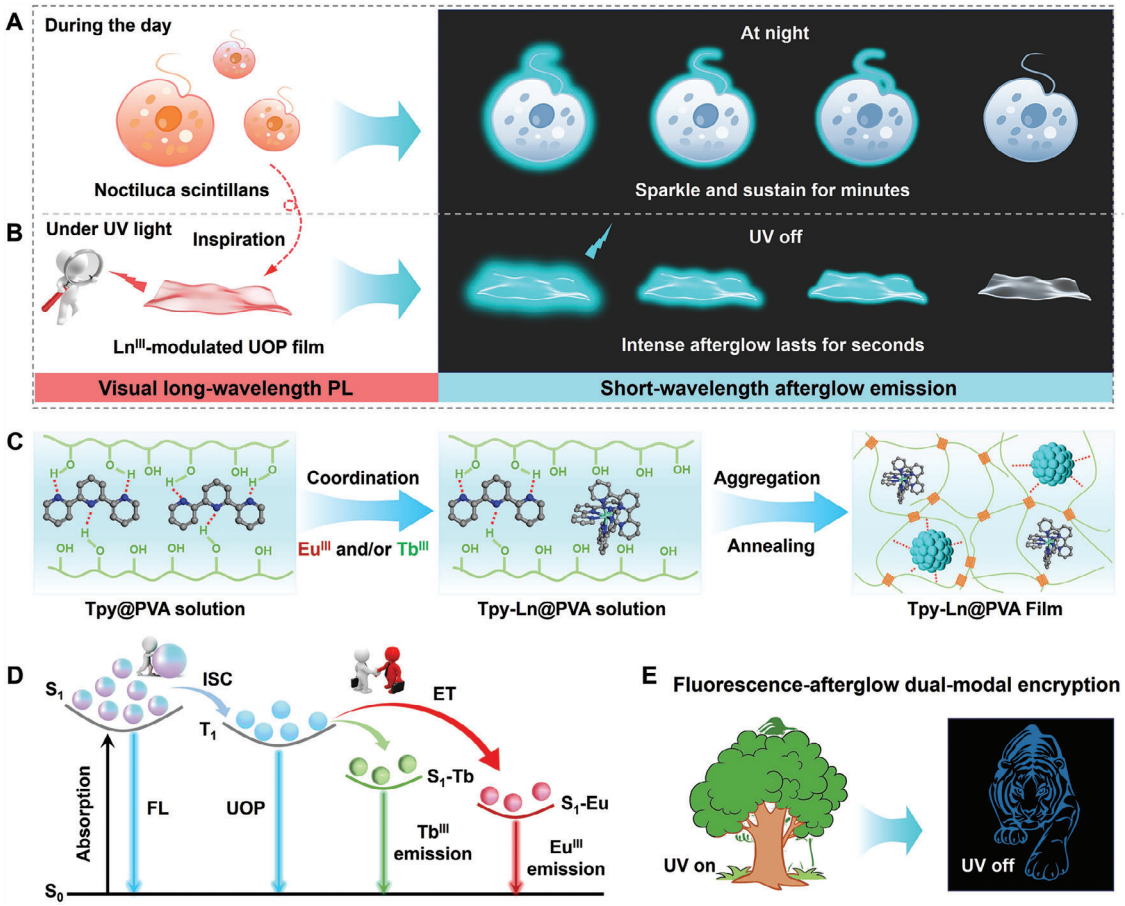

Scheme 1. A) Cartoon illustration of Noctiluca scintillans displaying red color during the day along with their cyan bioluminescence at night. B) Noctiluca scintillans-inspired Ln^{III}-modulated UOP films exhibits illusive long-wavelength fluorescence and short-wavelength afterglow emission. C) Schematic illustration of the preparation of Ln^{III}-modulated UOP films. D) Simplified Jablonski diagram for interpreting the emission mechanism of Ln^{III}-modulated UOP system. E) Fluorescence-afterglow dual-modal encryption system enabled by Ln^{III}-modulated UOP materials.

In recent years, ultralong organic phosphorescence (UOP), namely, afterglow emission has drawn intense research interest due to its fascinating optical phenomena.[10] Particularly, the intrinsic long-lived lifetime of UOP provides a unique time scale for information encryption and anti-counterfeiting, greatly enhancing the security of information storage.[11] Moreover, benefiting from their modulable afterglow lifetime and intensity, the newly-emerged UOP materials are capable of encoding more accessible information with high-level security and improved storage capacity.[12] However, it still remains challenging to precisely modulate UOP to achieve an elaborate afterglow gradient along with polychromatic fluorescence for developing fluorescence-afterglow dual-modal information encryption.

As one of the well-known bioluminescent creatures, the marine Noctiluca scintillans is a genus of dinoflagellates that generally displays red or green color during the day while it is scintillating with bright cyan color over minutes for communication and intimidating predators at night (**Scheme 1A**).[13] Inspired by such interesting phenomenon, we speculate whether it is possible to develop new optical materials with illusive emission phenomenon that fluorescence located at long wavelength but displaying the afterglow with short wavelength (Scheme 1B), which is highly appealing for innovative fluorescence-afterglow dual-modal encryption. To verify our hypothesis, we developed a hybrid optical system involving the introduction of 2,2′:6′,2″-terpyridine (Tpy) as organic phosphor as well as chelating ligand, and Ln^{III} as energy acceptor (Scheme 1C).[14] The Tpy phosphors can serve as an efficient organic antenna for sensitizing the luminescence of Ln^{III} after coordination, which is termed "antenna effect." That is, the energy can be transferred from triplet (T_1) states of Tpy ligand to the excited levels of the Ln^{III}, leading to efficient sensitized luminescence (Scheme 1D).[15] For one, the self-assembly of Tpy in PVA matrix leads to UOP emission owing to immense confinement provided by rigid environment and multiple hydrogen bonds from PVA. For another, the UOP emission can be further precisely modulated by the introduction of Ln^{III} coordination, providing multicolor fluorescence and UOP gradients on demand. As such, we envisage that it is possible to realize a unique coordination-modulated UOP system by combining Tpy phosphor and different Ln^{III} (Eu^{III} and/or Tb^{III}) in poly(vinyl alcohol) (PVA) matrix, which will contribute to fluorescence-afterglow dual-modal encryption (Scheme 1E). Such unique optical system enables camouflaging information by similar Ln^{III} fluorescence under UV light while deciphering information with

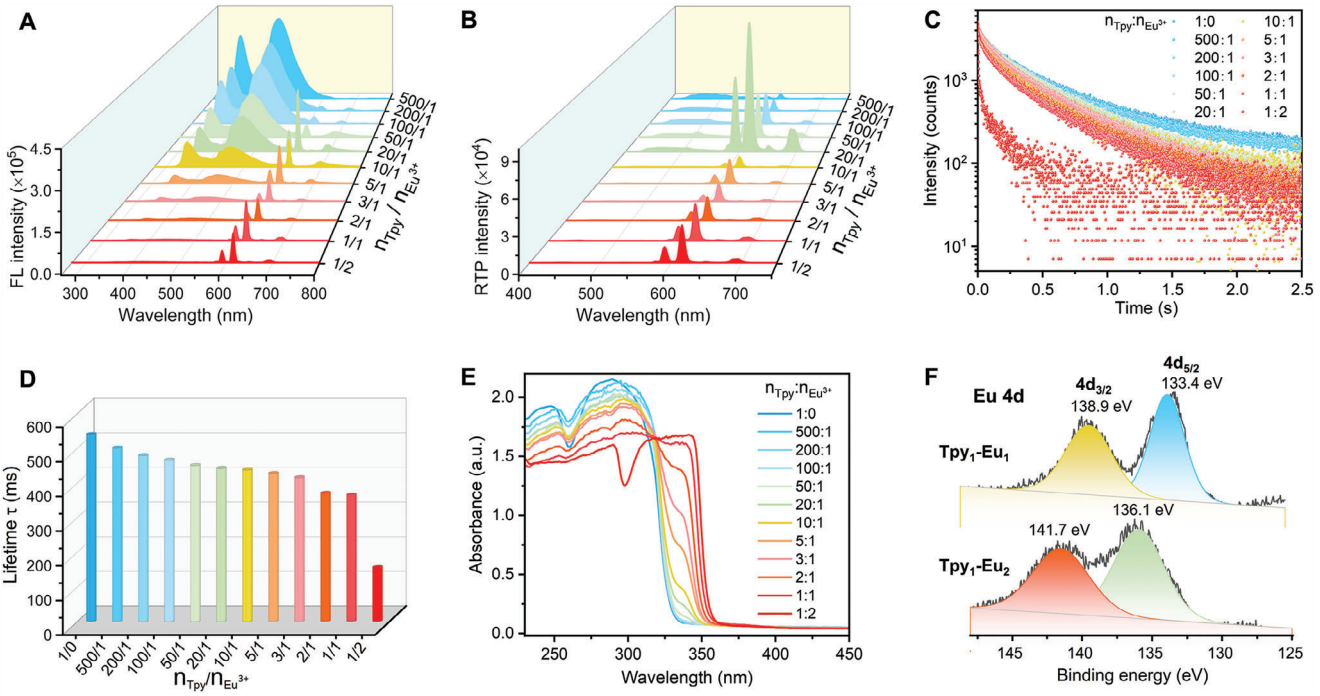

Figure 1. A) The steady-state (prompt) emission spectra of Eu^{III}-modulated UOP materials, λ_{ex} = 240 nm. B) Delayed emission spectra of Eu^{III}-modulated UOP materials, λ_{ex} = 240 nm, delayed 0.05 ms. C) Time-resolved emission-decay profile of Eu-modulated UOP materials, monitored at 485 nm. D) Phosphorescent lifetimes of Eu^{III}-modulated UOP materials. E) UV–vis absorption spectra of Eu^{III}-modulated UOP materials. F) Eu 4d XPS spectra of Tpy_1-Eu_1@PVA film (top), and Tpy_1-Eu_2@PVA film (bottom).

mutual afterglow. Moreover, the fluorescence and UOP performance including lifetime and intensity can be precisely regulated by adjusting doping ratio of Ln^{III} to access elaborate afterglow gradient on demand for spatial-time-resolved anti-counterfeiting applications. This unprecedented bio-inspired optical system is highly desirable for developing advanced fluorescence-afterglow dual-modal encryption including attacker-misleading information encryption and high-level anti-counterfeiting applications.

2. Result and Discussion

2.1. Fabrication and Characterization of Bio-Inspired Composite UOP Films

In this study, we aim to precisely modulate the UOP performance for fluorescence-afterglow dual-modal information encryption by metal-ligand (M-L) coordination. For this purpose, the Ln^{III}-doped UOP materials with different molar ratios of Ln^{III} (TPy_x-Ln_y@PVA, x/y denotes the molar ratio of Tpy to Ln^{III}) were facilely prepared in the first step by integrating Tpy phosphor with PVA matrix, followed by the introduction of Ln^{III}, which exhibited modulable ultralong persistent luminescence under ambient conditions (**Figure 1**). The purely organic afterglow material (Tpy@PVA) displays dual steady-state emission bands centered at 365 and 465 nm, and exhibits a prominent time-resolved emission peak at 485 nm with cyan afterglow about 3.0 s (Figures S1 and S2, Supporting Information). Thereafter, the Ln^{III} metal ions (Eu^{III} and/or Tb^{III}) were introduced into the Tpy@PVA UOP system to validate the idea that precisely tuning optical properties including fluorescence and phosphorescence via an efficient ET process. As expected, the prompt photoluminescence spectrum shows a consecutive decline of the intrinsic emission at 365 and 465 nm upon increasing the molar ratio of Ln^{III} dopant

(Figure 1a and Figure S3a, Supporting Information). It indicates that there is an efficient ligand-to-metal photosensitized energy transfer (PSET) between Tpy and Ln^{III}, which is also known as the "antenna effect" as depicted in Scheme 1D.[16] To confirm the PSET from Tpy phosphor to Ln^{III} acceptor, the steady-state lifetimes of Ln^{III}-modulated UOP materials were collected. The steady-state lifetimes of Tpy@PVA monitored at 365 and 465 nm are 2.02 and 4.30 ns, respectively (Figure S16, Supporting Information). It is found that the steady-state lifetimes are decreased slightly upon increasing Eu^{III} dopant up to 1:2 (Figure S17 and Table S1, Supporting Information), indicating minor ET from singlet state of Tpy to Ln^{III} may occur. Accordingly, the UOP at 485 nm follows the same trend with fluorescence emission showing gradually diminution (Figure 1b and Figure S3b, Supporting Information). Since the Ln^{III} luminescence has a phosphorescent lifetime of about 1.5 ms (Figure S4, Supporting Information), its delayed emission is still observed in the delayed emission spectra along with UOP. Accompanied by the decrease of afterglow intensity at 485 nm, the delayed emission of Eu^{III}-modulated UOP materials at 615 nm was increased to maximum and then decreased into a plateau, implying that the doping ratio for optimal sensitization efficiency is 20/1 (Tpy/Eu^{3+}, Figure S18, Supporting Information). However, the phosphorescent intensity of Tb^{III}-modulated UOP materials at 540 nm undergoes a continuous growth process until it reached a plateau, showing optimal sensitization efficiency at around 1/1 (Tpy/Tb^{3+}, Figure S18, Supporting Information). Thereby, the decline of afterglow emission

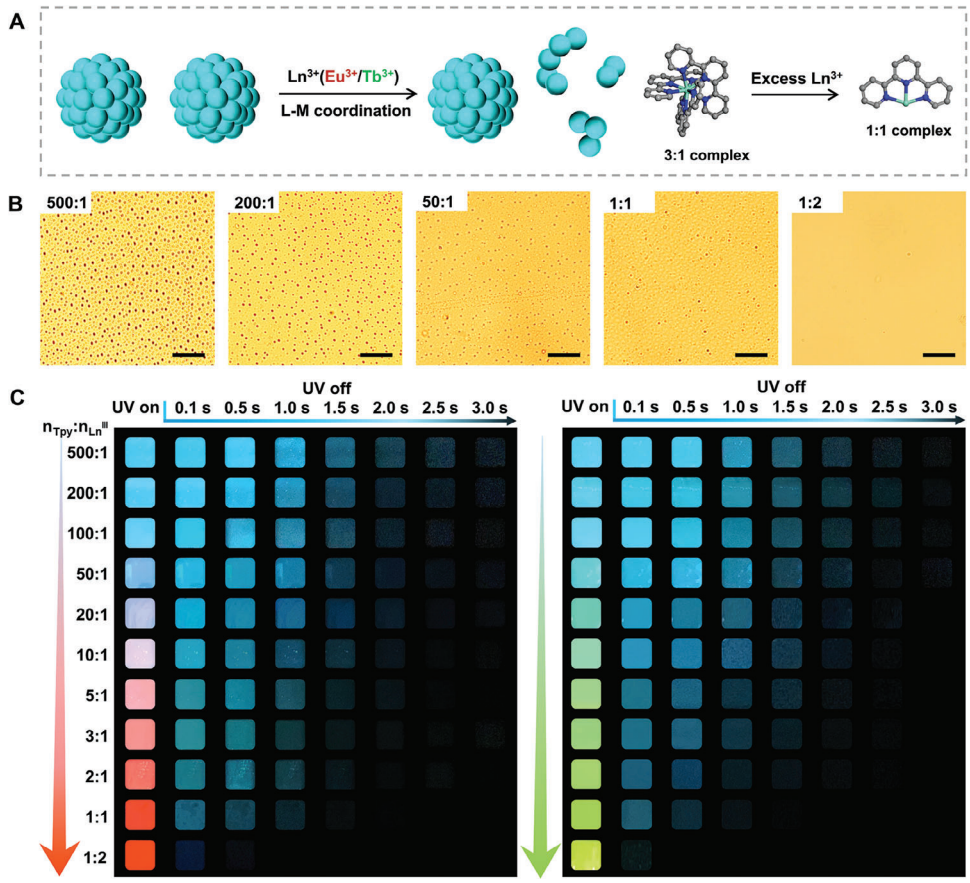

Figure 2. a) Schematic illustration of disassembly of Tpy aggregates and the coordination of Tpy molecules with Ln^{III} in the Tpy-Ln@PVA material systems. b) Optical microscopy (OM) images of Tpy-Eu@PVA with different doping ratios of Eu^{III}, scale bar 50 μm. c) Photographs of Ln-modulated UOP materials with different doping molar ratio of Eu^{III} (left) and Tb^{III} (right), the photos were taken under 254 nm UV excitation and at different time intervals after the removal of UV irradiation.

at 485 nm can be attributed to the PSET effect. As a result, the phosphorescent lifetime is also gradually reduced from 540 ms for Tpy@PVA to 156.2 ms for Tpy_1-Eu_2@PVA (Figure 1c,d) and 140.3 ms for Tpy_1-Tb_2@PVA (Figure S5, Supporting Information). Especially, it is found that the lifetime is decreased dramatically upon increasing molar ratio from 1:1 to 1:2 probably due to nearly complete coordination of Tpy molecules for Tpy_1-Ln_2@PVA systems. Given the significant variation of phosphorescent lifetime, the PSET from triplet state of Tpy phosphor to Ln^{III} should be a dominant pathway. In addition, the optimal phosphorescence quantum yields of these hybrid materials are 5.36% for Eu^{III}-modulated materials and 8.33% for Tb^{III}-modulated materials (Tables S2 and S3, Supporting Information), which are consistent with their delayed emission. As a comparison, the powders of $(Tpy)_3$-Ln^{III} complexes exhibit short-lived phosphorescence leads to no afterglow emission can be observed by naked eyes although they display strong luminescence under UV light (Figures S19 and S20, Supporting Information).

Along with the variation of coordination, the fluorescent color, afterglow intensity and duration were also capable of being precisely modulated (**Figure 2c**). Take Eu^{III}-doped UOP system for example, the fluorescent color changed from initial cyan to intense red and the afterglow intensity decreased continuously with duration declined from 3.0 s to 0.1s due to increasing PSET effect from Tpy phosphor to Eu^{III}. Especially, Tpy_1-Eu_1@PVA material exhibits much longer and stronger afterglow lasting over 1.5 s while Tpy_1-Eu_2@PVA displays only dim afterglow with duration of 0.1 s. It's worth noting that the afterglow emission of Eu^{III}- and Tb^{III}-modulated UOP materials is essentially identical due to the UOP originates from uncoordinated Tpy phosphors. Although the phosphorescence of Ln^{III} become dominant after the doping ratio is increased up to 50/1 (n_{Tpy}/n_{Ln}), the afterglow emission of Ln^{III} is not able to be observed by naked eyes due to their short-lived lifetime. Moreover, Eu^{III} and Tb^{III} were blended together to jointly tune the optical properties of UOP system. Interestingly, both Tpy-$Eu_{0.5}Tb_{0.5}$@PVA and Tpy-Eu_1Tb_1@PVA exhibit an intense yellow fluorescence owing to the superimposition of Eu^{III} and Tb^{III} luminescence (Figure S6, Supporting Information). Besides, the UOP performance of these two heterometal-doped materials matches with that of single Ln^{III} doped materials, revealing visible afterglow about 1.6 s for Tpy-$Eu_{0.5}Tb_{0.5}$@PVA while only weak and short afterglow can be observed by naked eyes for Tpy-Eu_1Tb_1@PVA (Figure S7, Supporting Information). In sharp contrast to those dye-doped materials, all UOP materials are highly transparent with transmittance of ≈90% (Figure S21, Supporting Information), which is beneficial to avoiding

information leakage under daylight. These results illustrate that both UOP performance (intensity and lifetime) and prompt luminescence can be finely modulated on-demand by varying the dopant ratio of Ln^{III}, which suggests great potential for a wide range of optical applications including high-level information encryption, anticounterfeiting and intelligent display.

To figure out the coordination modulation of afterglow, ultraviolet–visible (UV–vis) absorption spectroscopy and X-ray photoelectron spectroscopy (XPS) were fully implemented. As displayed in Figure 1e and Figure S8, Supporting Information, the shift of UV absorbance correlates well with the trend of UOP performance upon increasing molar ratio of Ln^{III} dopants. To be specific, the π-π* and n-π* transitions of Tpy molecules ranging from 230 to 300 nm become structureless accompanied by the gradual rise of absorbance at ≈350 nm for doping Eu^{III} (Figure 1e) and Tb^{III} (Figure S8, Supporting Information), which is attributed to the ligand-to-metal charge transfer (LMCT).[15a] The bathochromic shift and decrement of π-π* and n-π* absorbance bands indicate the isomerization of Tpy from *trans–trans* to *cis–cis* and the lone pair electrons of Tpy are delocalized to the empty orbital of the Ln^{III} upon complexation.[17] Concomitantly, the appearance and increase of LMCT absorbance at 350 nm can be observed owing to the increased ratio of coordination. Again, the sudden change in absorbance is observed at molar ratio of 1:2. Take Eu^{III}-doped UOP material as a model system, XPS experiments were employed to study such abrupt variation of optical properties. Through fitting analysis of Eu 4d, the peaks located at ≈138.9 ($4d_{3/2}$) and 133.4 eV ($4d_{5/2}$) for Tpy_1-Eu_1@PVA are significantly redshifted to 141.7 and 136.1 eV for Tpy_1-Eu_2@PVA (Figure 1f). Likewise, upshift of Eu 3d is observed from 1160.9 ($3d_{3/2}$) and 1131.6 eV ($3d_{5/2}$) for Tpy_1-Eu_1@PVA to 1161.7 and 1132.5 eV for Tpy_1-Eu_2@PVA (Figure S9, Supporting Information). Such similar shifts toward higher binding energy are probably attributed to the decrease of electron density from the change of binding mode as shown in Figure S9, Supporting Information. To be specific, intact complexes might be assembled in the case of Tpy_1-Ln_1@PVA due to a plethora of Tpy molecules. That is, there were still plenty of Tpy molecules uncoordinated with Ln^{III} due to diffusion of Ln^{III} in the PVA matrix, and thus visible intense UOP could be still observed. In this case, the empty orbitals of Ln^{III} are fully filled with lone pairs of Tpy to form intact 3:1 complex. However, 1:1 complexes can be formed in the case of excessive Ln^{III} for Tpy_1-Ln_2@PVA attributed to there is not sufficient Tpy molecules to form a thermodynamically stable 3:1 complex, leading to almost vanishment of UOP. These results demonstrate that the modulation of optical properties depends on the coordination between Tpy phosphor and Ln^{III}.

To further shed light on the modulation of UOP properties by coordination, optical microscopy (OM), small angle X-ray scattering (SAXS) and attenuated total reflectance-Fourier transform infrared (ATR-FTIR) spectroscopy were fully carried out. As depicted in Figure 2a, uniform microparticles with 2–3 μm can be observed owing to the self-assembly and aggregation of Tpy molecules in the PVA matrix. Upon the introduction of Ln^{III} dopant, the Tpy aggregates are depleted consecutively owing to the coordination of Tpy molecules with Ln^{III}. As a result, the phosphorescent intensity and lifetime of UOP system reveal gradually diminution. Besides, the SAXS results reveal that no significant change in structure at the nanoscale (Figure S10, Supporting Information). Moreover, the stretching vibrations of free pyridine ring (C═N, C═C) located at 1573.6 cm^{-1} for Tpy@PVA were almost vanished for Tpy_1-Ln_1@PVA and Tpy_1-Ln_2@PVA (Figure S11, Supporting Information), implying the introduction of dynamic coordination. These results demonstrate that the precise regulation of these Ln^{III}-doped UOP films resulted from coordination between Tpy molecules and Ln^{III}.

2.2. Precisely Modulated UOP for Multi-Level Information Encryption

In recent years, the UOP materials have exhibited outstanding applications in the fields of information encryption and anticounterfeiting.[18] The precise regulation of UOP performance on-demand to develop fluorescence-afterglow dual-modal information encryption is still challenging. Inspired by Noctiluca scintillans, we aim to develop innovative encryption system by using Ln^{III}-modulated UOP materials. As a proof-of-concept, a dot-matrix pattern (5 × 5) was fabricated for multi-level information encryption by selectively assembling Tpy_1-Eu_1@PVA, Tpy_1-Eu_2@PVA, Tpy_1-Tb_1@PVA and Tpy_1-Tb_2@PVA films (**Figure 3a**). The output of emissive dot is defined as "1" and non-emissive dot represents "0." which is comparable to binary data. Upon the UV light excitation, only disguised pattern is observed and no valid information can be obtained because all films emit intense fluorescence. However, the dot-matrix pattern represents a certain information after erasing UV source, which can be deciphered as "GOOD!" through given binary cipher (Table S4, Supporting Information) owing to the fast fadeout and weak of UOP afterglow for Tpy_1-Eu_2@PVA and Tpy_1-Tb_2@PVA films at the delay time of 0.1 s. It should be noted that we select such a delay time in order to eliminate the effect of short-lived Ln^{III} phosphorescence. Also, these Ln^{III}-modulated UOP materials can be well applied in the encryption of words and numbers by using similar fluorescence as camouflage with attacker-misleading ability (Figure S12a, Supporting Information). As displayed in Figure 3b and

Figure S12a, Supporting Information, when being exposed to 365 nm UV light, the obfuscate and misleading information of "8888" and "Sunrise" are masqueraded. However, the target information of "2023" and "Sun" can be deciphered, respectively, after stopping UV irradiation for 0.1 s (Videos S1 and S2, Supporting Information). More interestingly, the image of "lurking tiger" is appeared in the form of afterglow after the removal of UV excitation (Figure 3c and Figure S12b, Supporting Information). In this way, a new high-level information encryption method is successfully established by taking advantages of fluorescent information camouflage and decryption with afterglow display, revealing greatly improved crypticity and security.

To further validate our conception, we demonstrated a potential application of Ln^{III}-modulated UOP materials for multi-level information encryption as shown in the **Figure 4**. The "treasure map" was delicate designed and drawn with several Ln^{III}-modulated UOP materials (Figure S13, Supporting Information). In this encryption system, polychromatic fluorescence was employed to camouflage information for disorienting the treasure hunter, while the real information was hidden in the afterglow. Under daylight, no information can be obtained due to high

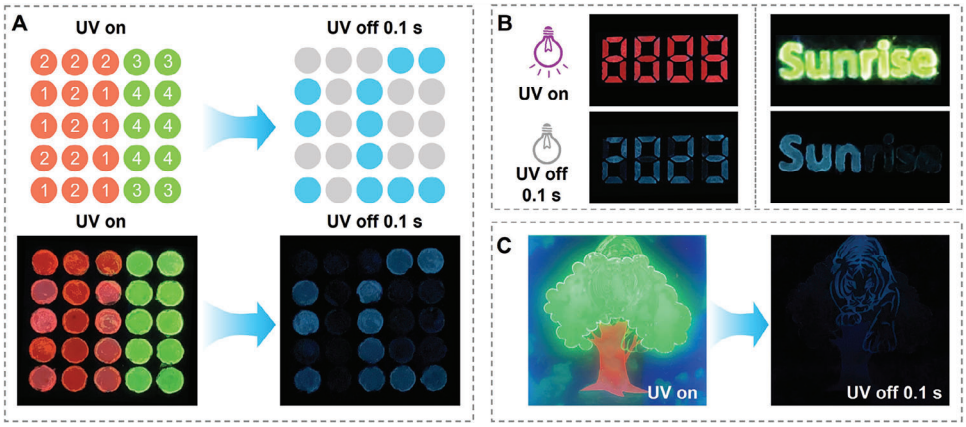

Figure 3. The multilevel encryption system by using fluorescence camouflage and decryption with UOP. A) Schematic illustration of a dot-matrix pattern, where "1" denotes Tpy_1-Eu_1@PVA, "2" denotes Tpy_1-Eu_2@PVA, "3" denotes Tpy_1-Tb_1@PVA, "4" denotes Tpy_1-Tb_2@PVA (top), the photos were taken under 254 nm UV light (bottom left) and after creasing excitation for 0.1 s (bottom right). B) The photos were taken under 254 nm UV light (top) and after creasing excitation for 0.1 s (bottom). C) The photos of "a lurking tiger" were taken under 254 nm UV light (left) and after creasing excitation the for 0.1 s (right).

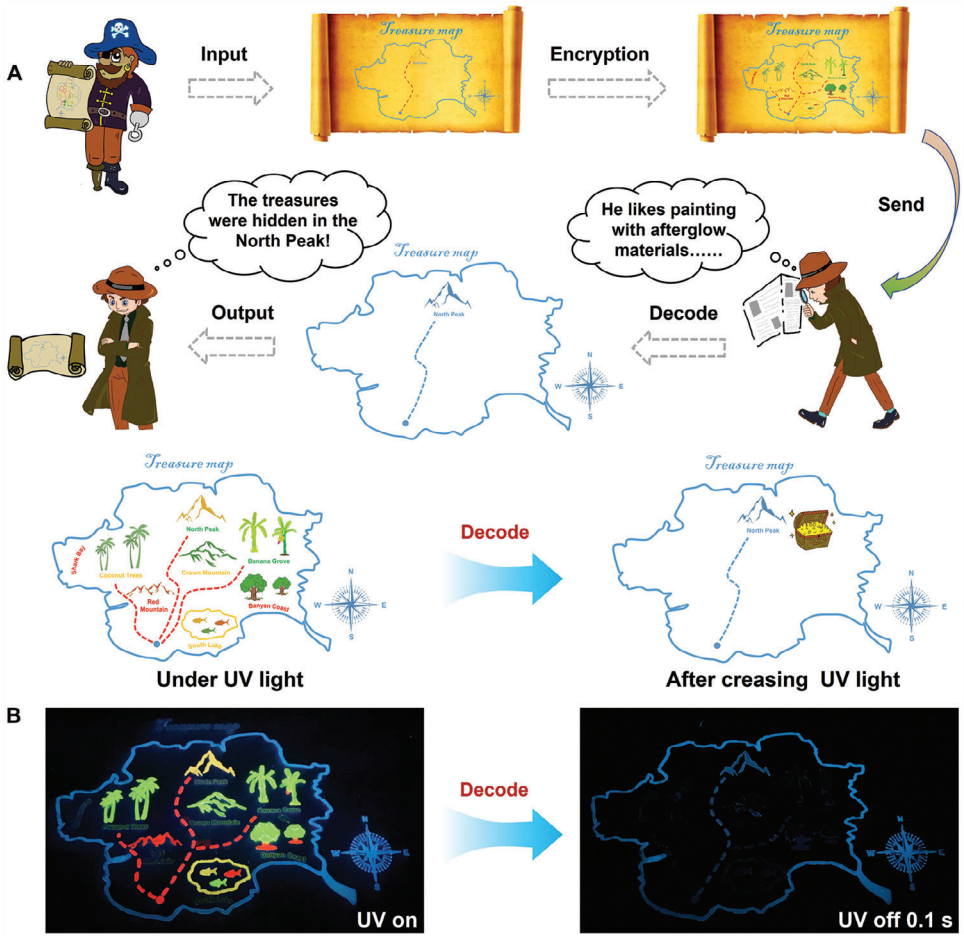

Figure 4. The multilevel encryption system of "treasure map". A) Diagram depicting the multi-level information encryption system for hiding target location of treasure. B) The photographs of "treasure map" 254 nm UV light (left) and after erasing UV irradiation (right) for 0.1 s.

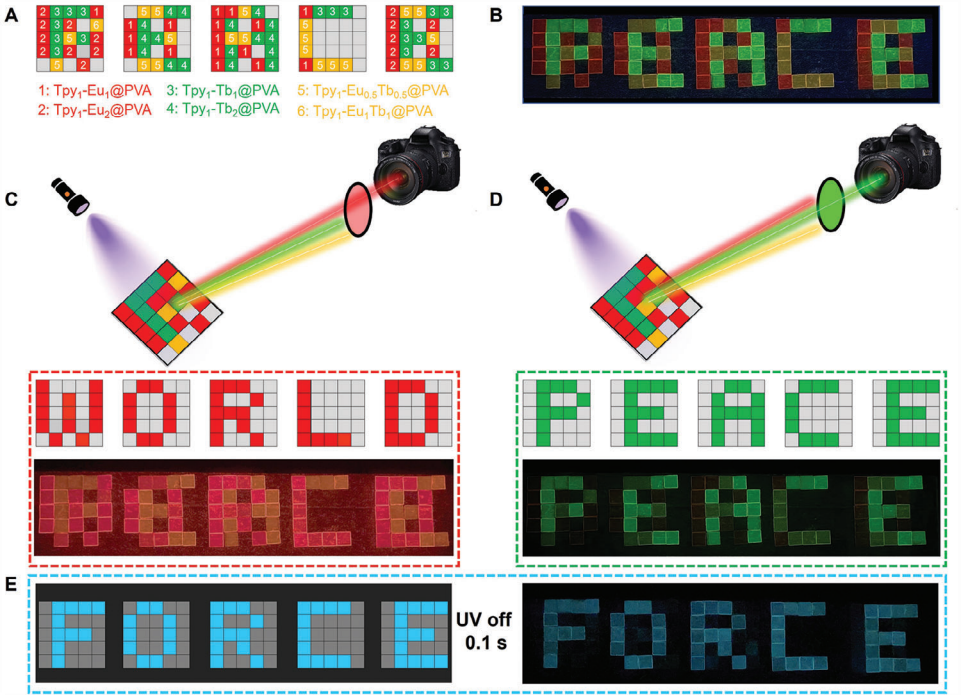

Figure 5. The illustration of the multi-level information output system. A) Schematic illustration of assembling complicated literal matrices by using mono- and double-Ln^{III}-modulated UOP materials. B) Digital image of literal matrices under 254 UV light. C) Schematic and digital images of the decoded "WORLD" under a red optical filter. D) Schematic and digital images of the decoded "PEACE" under a green optical filter. E) Schematic and digital images of the decoded "FORCE" after the removal of UV excitation for 0.1 s.

transparency of these Ln^{III}-modulated UOP materials (Figure S21, Supporting Information). Thereafter, a treasure map is presented with the assistance of UV irradiation, but the target location of the treasure is still hidden. After the removal of UV light for 0.1 s, the encrypted location of treasure on the map is appeared by visible afterglow (Video S3, Supporting Information). That is, the only way to know target information is to retrieve the correct key (fluorescence-afterglow dual-modal decryption).

Not only the innovative optical materials, but also the new techniques of encryption and decryption are necessary for enhancing high-level security.[19] Interestingly, plenty of marine fishes possess intraocular filters, which can function as hi-pass filters to render a specific range of wavelength to reduce chromatic aberration and dazzle, thus largely improving contrast vision.[20] The optical filters are also key components of various microscopes, cameras, and spectroscopic instruments, which are essential to obtain desired spectral band. Therefore, we speculated that whether it was possible to utilize optical filters to select the desired emission band to further improve the cryptographic security. A proof-of-concept demonstration is depicted in **Figure 5**, in which optical filters are used for selecting channels of fluorescence signals. For the sake of simplicity, five literal matrices were selectively assembled with six single- and double-Ln^{III}-modulated UOP materials for multi-level information encryption (Figure 5a). The Commission Internationale de l'Eclairage (CIE) 1931 coordinate diagram of these Ln^{III}-modulated UOP materials shows that there are three pairs of materials with similar colors (Figure S14, Supporting Information). Since three fluorescent colors are interfered with each other, the encrypted information is confusing and unable to be distinguished (Figure 5b). It is worth noting that the yellow fluorescence from Tpy_1-$Eu_{0.5}Tb_{0.5}$@PVA and Tpy_1-Eu_1Tb_1@PVA will provide information either red filter or green filter is performed due to the superimposition of Eu^{III} and Tb^{III} luminescence. As such, "WORLD" and "PEACE" can be identified with the help of red (600–700 nm) and green (500–600 nm) filters, respectively (Figure 5c,d and Videos S4 and S5, Supporting Information). Moreover, a deeper hidden information of "FORCE" can be decoded after creasing UV irradiation (Figure 5e and Video S6, Supporting Information). In this way, important information is camouflaged by polychromatic fluorescence, which can be decoded by specific optical filters. More importantly, a deeper level of information is further hidden in the afterglow, demonstrating high-level crypticity and security of information encryption.

2.3. Spatial-Time-Resolved Anti-Counterfeiting

The most of optical anti-counterfeiting techniques primarily rely on spatial-resolved variation, which faces high risk of being duplicated. To demonstrate our hypothesis of spatial-time-resolved anti-counterfeiting, we developed high-level anti-counterfeiting systems by the combination of various Ln^{III}-modulated UOP materials with lifetime gradient (**Figure 6**). As a conceptual demonstration, a faveolate pattern was designed as an anti-counterfeiting icon by assembling a family of Tb^{III}-modulated UOP films to verify the authenticity of honey (Figure 6a). Based on the afterglow gradient of these Ln^{III}-modulated UOP

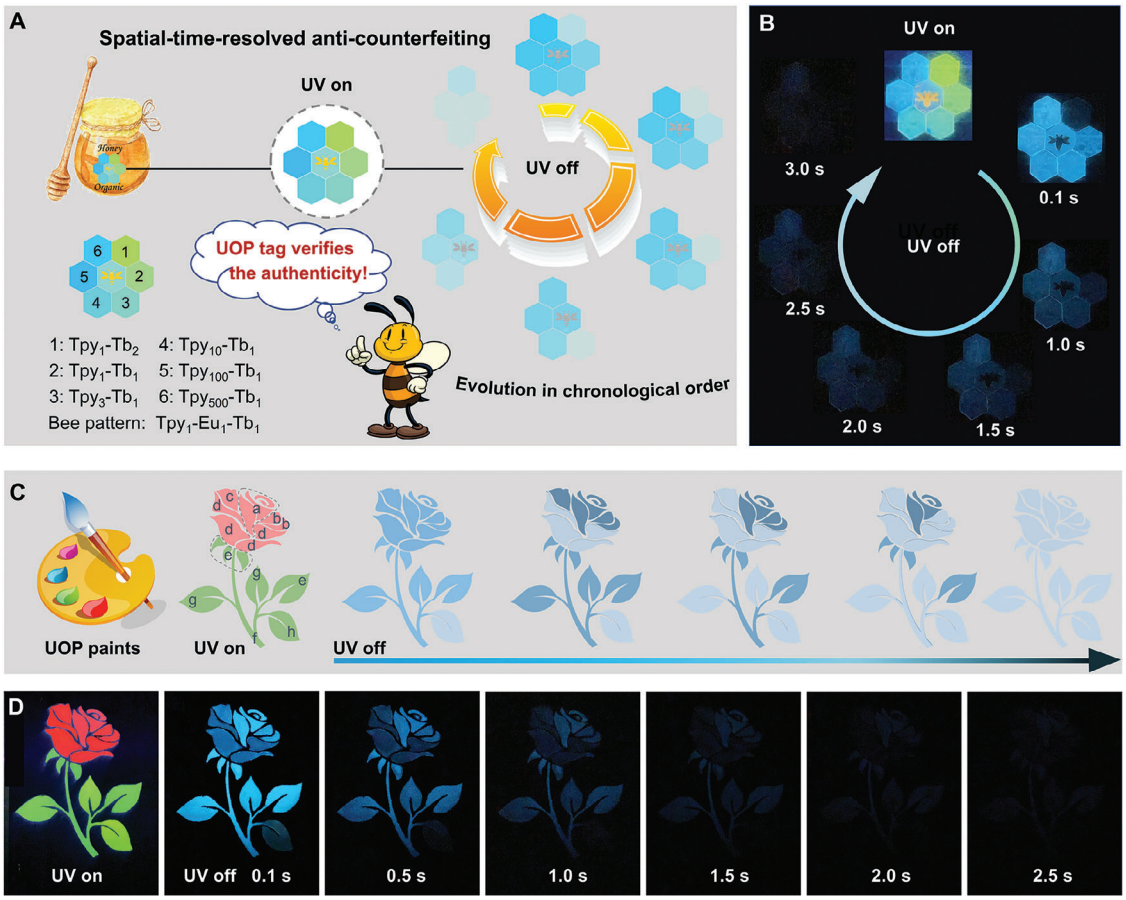

Figure 6. High-level spatial-time-resolved anti-counterfeiting applications. A) The schematic illustration of anti-counterfeiting icon for honey authentication by rationally assembling Tb^{III}-modulated UOP materials. B) Photographs of anti-counterfeiting faveolate pattern under 254 nm UV excitation and at different time intervals after erasing UV irradiation. C) The illustration of lifetime-coding for anti-counterfeiting by using Ln^{III}-modulated UOP as optical paints. D) The photographs of rose pattern under 254 nm UV excitation and its gradual withering in chronological order after the removal of excitation source.

materials, spatial-time-dependent revolution of the faveolate pattern would be displayed. As shown in Figure 6b and Video S7, Supporting Information, a vivid faveolate icon with a bee pattern at the center is appeared under UV light. Then, the hexagon and bee pattern that made by Tpy_1-Tb_2@PVA and Tpy_1-Eu_1-Tb_1@PVA, respectively, disappeared immediately at 0.1 s after the removal of UV excitation source. The other hexagon units fade away in a clockwise order due to longer lifetime of less Ln^{III}-doped

UOP materials. By this means, spatial-time-resolved anti-counterfeiting systems are successfully realized with high security level, which arehighly appealing for the identification of authentic commodities. Furthermore, Eu^{III}- and Tb^{III}-doped UOP materials were jointly used as colorful paints for high-level anti-counterfeiting (Figure 6c and Figure S15, Supporting Information). In this case, we selected a model pattern of rose to illustrate our design idea for anti-counterfeiting applications. To be specific, the different parts of the rose pattern painted with different Ln-modulated UOP materials with afterglow gradient would fade away in chronological order. Indeed, the rose painting seems to be wilting after creasing UV light in addition to vivid rose pattern under UV light (Figure 6d and Video S8, Supporting Information). The leaf pattern made by Tpy_1-Tb_2@PVA were the first to fade away while the petals and leaves painted with Tpy_5-Eu_1@PVA and Tpy_5-Tb_1@PVA vanished finally at 2.5 s. Compared with the common optical methods used for anti-counterfeiting, this spatial-time-resolved anti-counterfeiting strategy manifests largely improved security to verify the authenticity without complicated device and tedious material preparation.

3. Conclusion

Inspired by the Noctiluca scintillans, we have presented a feasible and reliable approach that combined lanthanide luminescence for camouflaging information and coordination-modulated UOP for deciphering target information, yielding greatly improved crypticity and security. A new strategy to precisely modulate the optical properties of UOP materials based on Ln^{III} coordination is developed, which manifests a powerful ability to tune UOP performance on-demand for high-level encryption and anti-counterfeiting applications. It was found that both lifetime and phosphorescent intensity can be finely modulated via Ln^{III} coordination based on efficient energy transfer. As a result, the

afterglow duration was effectively tuned varying from 3.0 s to 0.1 s along with diversified fluorescent color were successfully achieved. Benefiting from precisely modulated UOP and polychromatic fluorescence, multilevel information encryption systems were established by providing misleading and illusive information with polychromatic emission and deciphering information with mutual cyan afterglow, largely enhancing the related crypticity and security. In addition, multilevel information could be decrypted with the help of optical filters and switching UV excitation, which not only improved the information storage capacity but also facilitated the high-level information encryption. More importantly, spatial-time-resolved anti-counterfeiting systems were well established by using Ln^{III}-modulated UOP materials with afterglow gradient for authentication with high security. These findings were ingeniously leveraged to demonstrate advanced applications including high-level information encryption and anti-counterfeiting.

4. Experimental Section

Materials: Polyvinyl alcohol 1799 (PVA 99, ≈98–99% hydrolyzed degree) was purchased from Aladdin Chemistry Co. Ltd. 2,2′:6′,2′-Terpyridine and $Tb(NO_3)_3{\cdot}5H_2O$ (99.9%), purchased from Aladdin Chemistry Co. Ltd. $Eu(NO_3)_3{\cdot}6H_2O$ (99.9%) was supplied by Energy Chemical. The red optical filter (centered at a wavelength of 650 nm ± 20 nm) and green optical filter (green: 500–600 nm) were purchased from Shenzhen Huateng Vision and CHENGXINLI CO., respectively.

Preparation of Ln^{III}-Modulated UOP Materials: The Tpy_x-Ln_y@PVA film (x/y refer to the molar ratio of Tpy to Ln^{III}) were fabricated by a simple drop-casting and annealing method. Take the Tpy_1-Eu_1@PVA film (the molar ratio of Tpy to Ln^{III} = 1:1) for example: The mixed solution of Tpy (5.0 mg, 0.021 mmol), $Eu(NO_3)_3{\cdot}6H_2O$ (9.6 mg, 0.021 mmol) and PVA (500 mg, 99% hydrolyzed degree) in water (7.0 mL) were stirred at 96 °C for 45 min to obtain homogeneous precursor solution. The resulted precursor solution was free standing for thermal annealing immediately at 65 °C for 15 min. Subsequently, 2.0 mL of the obtained aqueous precursor solution was taken and drop-casted on the cover glass (25 mm × 75 mm) with a pipette. Finally, the cover glass was then evaporated at 65 °C for 1 h to obtain Tpy_1-Eu_1@PVA film with thickness of about 100 µm. The fabrication method of the other lanthanide-doped UOP films is similar to that described above. (Notes for coordination process: Tpy molecules, Ln^{III} and PVA are well dispersed in water to form homogeneous solution at 96 °C; Then, the Tpy molecules as an NNN-type Pincer ligand are prone to coordinate with Ln^{III} at 65 °C to form thermodynamically stable metal-organic complexes. In this process, geometry of Tpy is converted from *trans–trans* to *cis–cis* lead to co-planar conformation of pyridine units for metal chelation.)

Characterization: UV–vis absorption and transmittance spectra were recorded on a UV–vis spectrophotometer (TU-1810, Purkinje General Instrument Co., Ltd). ATR-FTIR was performed with Cary660 FTIR spectrometer. The small angle X-ray scattering (SAXS) patterns were carried out with Xeuss 3.0. Steady-state fluorescence, time-resolved (delayed) emission and time-resolved emission-decay measurements were measured by a FL3-111 fluorescence spectrofluorometer at room temperature. Absolute quantum yields were determined by integrating the sphere on a Quantum Yield test system (QE-2100). The lifetime (τ) of the emission was obtained by fitting the decay curve with a multiexponential decay function:

$$I(t) = \sum_i A_i e^{-\frac{t}{\tau_i}} \quad (1)$$

where A_i and τ_i represent the amplitude and lifetime of an individual component for multiexponential decay profiles, respectively.

The average lifetimes were calculated according to the following equation:

$$\tau_{avg} = \sum \alpha_i \tau_i^2 / \alpha_i \tau_i \quad (2)$$

Supporting Information

Supporting Information is available from the Wiley Online Library or from the author.

Acknowledgements

This project was financially supported by the National Key Research and Development Program of China (2022YFB3204301), the National Natural Science Foundation of China (22205249), China Postdoctoral Science Foundation (2021TQ0341, 2022M723252), Zhejiang Provincial Natural Science Foundation of China (LQ23B040002), Natural Science Foundation of Ningbo (2021J203), Foundation of the Director of NIMTE (2021SZKY0305).

Conflict of Interest

The authors declare no conflict of interest.

Data Availability Statement

Research data are not shared.

Keywords

anticounterfeiting, biomimetics, coordination-modulated, information encryption, ultralong organic phosphorescence

Received: August 23, 2023
Revised: November 30, 2023
Published online:

[1] a) D. Cyranoski, *Nature* **2017**, *545*, 148; b) R. Arppe, T. J. Sørensen, *Nat. Rev. Chem.* **2017**, *1*, 0031.
[2] BASCAP, INTA, The Economic Impacts of Counterfeiting and Piracy. Frontier Economics, http://www.inta.org (accessed: 2017).
[3] World Health Organization IMPACT, Counterfeit medicines: and update on estimates, http://www.who.int/medicines/services/counterfeit/impact/TheNewEstimatesCounterfeit.pdf (accessed: 2006)
[4] a) P. She, Y. Ma, Y. Qin, M. Xie, F. Li, S. Liu, W. Huang, Q. Zhao, *Matter* **2019**, *1*, 1644; b) T. Ma, T. Li, L. Zhou, X. Ma, J. Yin, X. Jiang, *Nat. Commun.* **2020**, *11*, 1811; c) X. Le, H. Shang, H. Yan, J. Zhang, W. Lu, M. Liu, L. Wang, G. Lu, Q. Xue, T. Chen, *Angew. Chem., Int. Ed.* **2021**, *60*, 3640; d) Y. Yang, Q. Li, H. Zhang, H. Liu, X. Ji, B. Z. Tang, *Adv. Mater.* **2021**, *33*, 2105418.
[5] W. Ye, F. Zeuner, X. Li, B. Reineke, S. He, C.-W. Qiu, J. Liu, Y. Wang, S. Zhang, T. Zentgraf, *Nat. Commun.* **2016**, *7*, 11930.
[6] H. Hu, H. Zhong, C. Chen, Q. Chen, *J. Mater. Chem. C* **2014**, *2*, 3695.
[7] a) Y. Sun, X. Le, S. Zhou, T. Chen, *Adv. Mater.* **2022**, *34*, 2201262; b) H. Yang, K. Ou, H. Wan, Y. Hu, Z. Wei, H. Jia, X. Cheng, N. Liu, H. Duan, *Mater. Today* **2023**, *67*, 424.

[8] a) O. Guillou, C. Daiguebonne, G. Calvez, K. Bernot, *Acc. Chem. Res.* **2016**, *49*, 844; b) S. Wei, W. Lu, X. Le, C. Ma, H. Lin, B. Wu, J. Zhang, P. Theato, T. Chen, *Angew. Chem., Int. Ed.* **2019**, *58*, 16243; c) H. Shi, S. Wu, M. Si, S. Wei, G. Lin, H. Liu, W. Xie, W. Lu, T. Chen, *Adv. Mater.* **2022**, *34*, 2107452; d) Y. Xie, Y. Song, G. Sun, P. Hu, A. Bednarkiewicz, L. Sun, *Light Sci. Appl.* **2022**, *11*, 150.

[9] J. Liu, H. Rijckaert, M. Zeng, K. Haustraete, B. Laforce, L. Vincze, I. Van Driessche, A. M. Kaczmarek, R. Van Deun, *Adv. Funct. Mater.* **2018**, *28*, 1707365.

[10] a) Z. An, C. Zheng, Y. Tao, R. Chen, H. Shi, T. Chen, Z. Wang, H. Li, R. Deng, X. Liu, W. Huang, *Nat. Mater.* **2015**, *14*, 685; b) S. Xu, R. Chen, C. Zheng, W. Huang, *Adv. Mater.* **2016**, *28*, 9920; c) R. Kabe, C. Adachi, *Nature* **2017**, *550*, 384; d) X. Ma, J. Wang, H. Tian, *Acc. Chem. Res.* **2019**, *52*, 738; e) Q. Wang, X. Dou, X. Chen, Z. Zhao, S. Wang, Y. Wang, K. Sui, Y. Tan, Y. Gong, Y. Zhang, W. Z. Yuan, *Angew. Chem., Int. Ed.* **2019**, *58*, 12667; f) W. Ye, H. Ma, H. Shi, H. Wang, A. Lv, L. Bian, M. Zhang, C. Ma, K. Ling, M. Gu, Y. Mao, X. Yao, C. Gao, K. Shen, W. Jia, J. Zhi, S. Cai, Z. Song, J. Li, Y. Zhang, S. Lu, K. Liu, C. Dong, Q. Wang, Y. Zhou, W. Yao, Y. Zhang, H. Zhang, Z. Zhang, X. Hang, et al., *Nat. Mater.* **2021**, *20*, 1539; g) H. Shi, W. Yao, W. Ye, H. Ma, W. Huang, Z. An, *Acc. Chem. Res.* **2022**, *55*, 3445.

[11] a) Y. Wang, J. Yang, M. Fang, Y. Yu, B. Zou, L. Wang, Y. Tian, J. Cheng, B. Z. Tang, Z. Li, *Matter* **2020**, *3*, 449; b) R. Tian, S.-M. Xu, Q. Xu, C. Lu, *Sci. Adv.* **2020**, *6*, eaaz6107; c) D. Li, J. Yang, M. Fang, B. Z. Tang, Z. Li, *Sci. Adv.* **2022**, *8*, eabl8392; d) T. Chen, Y.-J. Ma, D. Yan, *Adv. Funct. Mater.* **2023**, *33*, 2214962.

[12] a) W. Zhao, Z. He, B. Z. Tang, *Nat. Rev. Mater.* **2020**, *5*, 869; b) P. Wei, X. Zhang, J. Liu, G.-G. Shan, H. Zhang, J. Qi, W. Zhao, H. H.-Y. Sung, I. D. Williams, J. W. Y. Lam, B. Z. Tang, *Angew. Chem., Int. Ed.* **2020**, *59*, 9293; c) H. Peng, G. Xie, Y. Cao, L. Zhang, X. Yan, X. Zhang, S. Miao, Y. Tao, H. Li, C. Zheng, W. Huang, R. Chen, *Sci. Adv.* **2022**, *8*, eabk2925; d) W. Dai, G. Li, Y. Zhang, Y. Ren, Y. Lei, J. Shi, B. Tong, Z. Cai, Y. Dong, *Adv. Funct. Mater.* **2022**, *33*, 2210102; e) Y. Zhang, Q. Sun, L. Yue, Y. Wang, S. Cui, H. Zhang, S. Xue, W. Yang, *Adv. Sci.* **2022**, *9*, 2103402; f) W.-L. Zhou, W. Lin, Y. Chen, X.-Y. Dai, Y. Liu, *Small* **2023**, *19*, 2304009; g) Y.-Y. Hu, X.-Y. Dai, X. Dong, M. Huo, Y. Liu, *Angew. Chem., Int. Ed.* **2022**, *61*, 202213097; h) Z. Chen, X. Chen, D. Ma, Z. Mao, J. Zhao, Z. Chi, *J. Am. Chem. Soc.* **2023**, *145*, 16748.

[13] S. M. E. Smith, D. Morgan, B. Musset, V. V. Cherny, A. R. Place, J. W. Hastings, T. E. Decoursey, *Proc. Natl. Acad. Sci. U. S. A.* **2011**, *108*, 18162.

[14] a) R. Shunmugam, G. N. Tew, *J. Am. Chem. Soc.* **2005**, *127*, 13567; b) P. Chen, Q. Li, S. Grindy, N. Holten-Andersen, *J. Am. Chem. Soc.* **2015**, *137*, 11590; c) Y. Zhou, H.-Y. Zhang, Z.-Y. Zhang, Y. Liu, *J. Am. Chem. Soc.* **2017**, *139*, 7168; d) G. Yin, W. Lu, J. Huang, R. Li, D. Liu, L. Li, R. Zhou, G. Huo, T. Chen, *Aggregate* **2023**, *4*, e344.

[15] a) W. M. Faustino, O. L. Malta, G. F. De Sá, *J. Chem. Phys.* **2005**, *122*, 54109; b) J. Feng, H. Zhang, *Chem. Soc. Rev.* **2013**, *42*, 387; c) M. C. Heffern, L. M. Matosziuk, T. J. Meade, *Chem. Rev.* **2014**, *114*, 4496; d) W. Thor, Y. Wu, L. Wang, Y. Zhang, P. A. Tanner, K.-L. Wong, *Nat. Commun.* **2021**, *12*, 6532.

[16] N. Sabbatini, M. Guardigli, J.-M. Lehn, *Coord. Chem. Rev.* **1993**, *123*, 201.

[17] L. J. Charbonnière, S. Mameri, D. Flot, F. Waltz, C. Zandanel, R. F. Ziessel, *Dalton Trans.* **2007**, 2245.

[18] J. Zhang, S. Xu, L. Zhang, X. Wang, Y. Bian, S. Tang, R. Zhang, Y. Tao, W. Huang, R. Chen, *Adv. Mater.* **2022**, *34*, 2206712.

[19] a) S. Miao, Y. Wang, L. Sun, Y. Zhao, *Nat. Commun.* **2022**, *13*, 4044; b) F. Bian, L. Sun, L. Cai, Y. Wang, Y. Zhao, *Proc. Natl. Acad. Sci. U. S. A.* **2020**, *117*, 22736; c) Y. Liu, S. Liang, C. Yuan, A. Best, M. Kappl, K. Koynov, H.-J. Butt, S. Wu, *Adv. Funct. Mater.* **2021**, *31*, 2103908.

[20] a) P. H. Heinermann, *Exp. Biol.* **1984**, *43*, 127; b) J. S. Sparks, R. C. Schelly, W. L. Smith, M. P. Davis, D. Tchernov, V. A. Pieribone, D. F. Gruber, *PLoS One* **2014**, *9*, 83259.